# Computational design of cutin derivative bio-materials from fatty acids

9

*Otto V.M. Bueno*[a], *Jose J. Benitez*[b], *and Miguel A. San-Miguel*[a]
[a]Department of Physical Chemistry, Institute of Chemistry, University of Campinas, Campinas, Brazil, [b]Instituto de Ciencias de Materiales de Sevilla, Centro Mixto CSIC-Universidad de Sevilla, Sevilla, Spain

## 1 Introduction

### 1.1 Green materials

Due to current environmental problems, the development and use of green materials have become a necessity in our daily lives. Green materials are abundant in nature and offer unique properties, including non-toxicity and biodegradability, which are highly desired for sustainable development. This chapter aims at describing the latest studies on the behaviour of polyhydroxylated fatty acids as a source for green materials. It also demonstrates that the use of theoretical methods allied to experimental surface characterization techniques is a valuable tool to gain insight into the fundamental physical-chemical processes, and to better understand the mechanisms involved in the design and fabrication of green materials.

### 1.2 Biomimetics

Biomimetics is a research area that studies the phenomena and processes of nature with the aim of understanding them and then being able to use and modify their mechanisms for the benefit of society [1]. One of the oldest manufactured and patented materials based on this concept is Velcro (Fig. 1A). The developer of this material (Swiss engineer Georges de Mestral, 1907) observed that the burr seeds got attached to his pet during its routine walk. His experience as a researcher and his knowledge about microscopy led him to note that the seeds of these plants have intertwined strands with small hooks at the tip (Fig. 1B). Using this observation, he was able to apply this same reasoning to manufacture materials with those same characteristics, giving rise to Velcro materials. This material was then widely improved and used in the textile industry.

Specifically, biomimetics focuses on learning from biological systems and applying the gained knowledge in different domains of science. Therefore, biomimetics has a multidisciplinary approach that connects several areas of science with nature and allows the obtainment of materials with innovative properties [2].

**Green Chemistry and Computational Chemistry.** https://doi.org/10.1016/B978-0-12-819879-7.00001-5

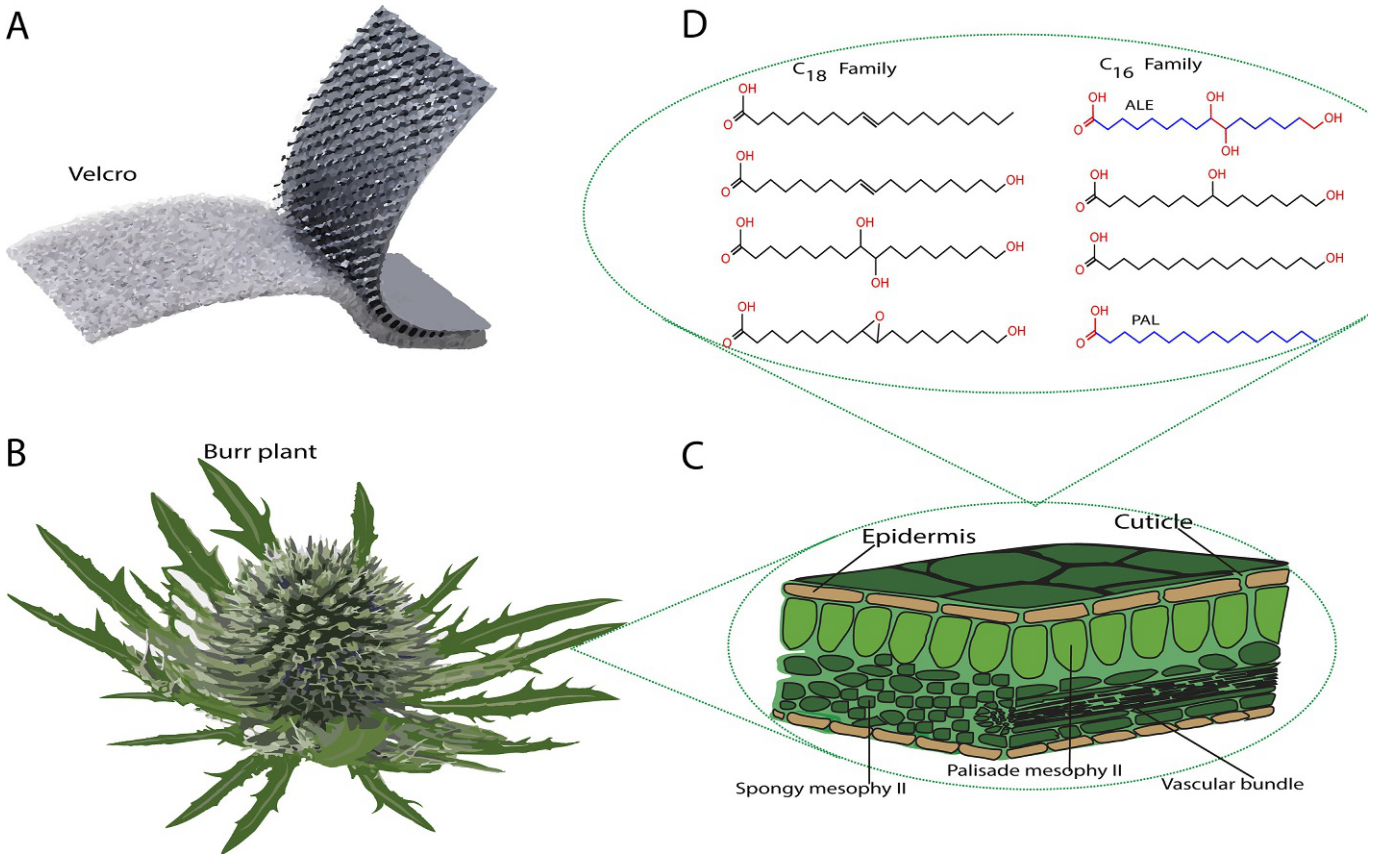


**Fig. 1** Graphic illustrations of processes involving biomimetics. (A) Image of Velcro: one of the first materials manufactured using the concept of biomimetics. (B) Arctium plant (burdock); the creation of Velcro was inspired by this plant. (C) A typical leaf cross-section showing the location of cutin and other components of the epidermal cell. (D) Major polyhydroxy fatty acid monomers located in cutin.

Numerous examples can illustrate this idea. For instance, nylon fibres—whose main characteristic is their high resistance—were inspired by spider webs. The possibility of nylon fibres with chemical modification enabling them to achieve strength equivalent to metal cables is being investigated [3]. Another important material is biodegradable plastics that can decompose in a short time. The creation of these plastics was inspired by the mechanism of the degradation caused by bacteria [4, 5].

This chapter focuses specifically on the biomimetics of cutin biopolymer present in plant epidermal cells. Their structural and chemical behaviour is shown when they are deposited on a flat support without forming chemical bonds with the surface.

## 1.3 Cutin-related biopolymers

Biopolyester cutin is an essential part of the barrier tissues of vegetables [6]. The outer part of vegetables is covered by a cell membrane named 'epidermal cell' (Fig. 1C). The epidermal cell is a set of cells of varied shapes and functions, covering the primary body of plants, leaves, flowers, roots, and stem [7]. The epidermal cells secret waterproofing substances that form coating films called cuticle [8]. Cutin is the main component of the cuticle [8]. The thickness and structure of the cuticle change markedly during the growth and development of the plant. These changes are correlated with changes in the composition of cutin [9]. Therefore, cutin can be considered a protective interface between the plant and the environment, minimizing the impact of pathogen-induced deterioration [7]. Cutin is embedded and coated with intracuticular and epicuticular waxes, respectively, forming complex mixtures of hydrophobic material containing long-chain fatty acids [7]. The combination of cutin, waxes, and polysaccharides creates the cuticle [8].

The chemical composition of cutin varies greatly among plants. Cutin consists of esterified monomers. The main monomers are poly-hydroxylated carboxylic acids with 16 and 18 carbon atoms in the aliphatic chain, normally classified as $C_{16}$ and $C_{18}$ families, respectively (Fig. 1D). In the initial stages of cutin development, the formation of well-organized laminar structures is observed, named procutin. In advanced stages, the laminar arrangement is lost to give way to reticulated and amorphous forms [10].

The synthesis of these monomers, using a variety of chemical methods, has widely been reported. The most used methods are based on hydroxylation and epoxidation reactions, all catalysed by oxygen or enzyme systems [11–15].

In the present decade, the monomers of the $C_{16}$ family were widely studied, to obtain biomimetic materials, focusing on properties such as biodegradability and non-toxicity [16]. Specifically, these studies are based on understanding the role of hydroxyl groups (primary and secondary) and their effect on the self-assembling process [16].

Theoretical and experimental studies show that hydroxyl groups in the middle of the aliphatic chain favour the growth of 2D networks, forming homogeneous monolayers. When the hydroxyl groups are located at terminal positions, they favour 3D growth forming layers of different thicknesses and nanoparticles [17]. All theoretical studies carried out so far confirm that the location and quantity of hydroxyl groups in

the aliphatic chain of cutin monomers define their macroscopic behaviour, which was confirmed by experimental techniques such as transmission electron microscopy (TEM) [18] and atomic force microscopy (AFM) [19]. All these studies show that carboxylic groups strategically located in the aliphatic chain lead to self-assembled systems.

This chapter unfolds the latest research to better understand self-assembly behaviour. Specifically, it focuses on the behaviour of aleuritic acid (ALE) and palmitic acid (PAL) monomers because they represent two fundamental molecular models. Both molecules adsorb to the surface through the terminal carboxylic group. ALE also has one terminal and two lateral hydroxyl groups, becoming a representative monomer for the maximization of intermolecular interactions to form 2D and 3D networks [20]. On the contrary, PAL has no hydroxyl groups and has been used in other studies as a reference molecule to compare with.

## 1.4 Self-assembly behaviour

Self-assembly is a recurring mechanism in nature to build highly complex structures. The common supports where this behaviour is observed are metal oxides and metals such as gold, platinum, silver, etc. [21]. The self-assembly behaviour on these supports (noted, for example, when depositing organic molecules on them) is due to the formation of covalent bonds formed between the surface atoms of the support and the organic molecule [22]. One of the most studied cases is that of gold support forming covalent bonds with the sulphur atoms of the thiol groups [22] (Fig. 2). The formation of covalent bonds between the organic molecules and the support in many cases largely influences the self-assembly process [23, 24].

On the other hand, the self-assembled laminar behaviour observed in the first stages of cutin formation does not require any type of support. In these cases, the self-assembly behaviour intrinsically depends on the structures of the cutin monomers and is not conditioned by any type of external inorganic support. For that reason, it is important to use a chemically inert support to guarantee minimal influence on the self-assembly process, just to allow effective lateral interactions between the adsorbates; in other words, the support does not have to form covalent bonds or H-bonds with the adsorbates. Different support models that satisfy these conditions can be used to carry out the theoretical studies with molecular dynamics (MD) simulations.

## 1.5 Selection of the support

Mica has been chosen and used as an ideal support to conduct studies on the behaviour of cutin monomers in many systems. The use of mica prevents the formation of covalent bonds and also ensures that the intermolecular forces between the mica and the cutin monomers are much weaker than between the monomers. Mica supports proved to be an excellent option because they can be readily cleaved on flat and atomically clean surfaces [16]. Muscovite is the most abundant mica and one of the most chemically stable minerals. Its chemical formula is $(KAl_2(AlSi_3O_{10})(OH)_2)$ [25]. In the

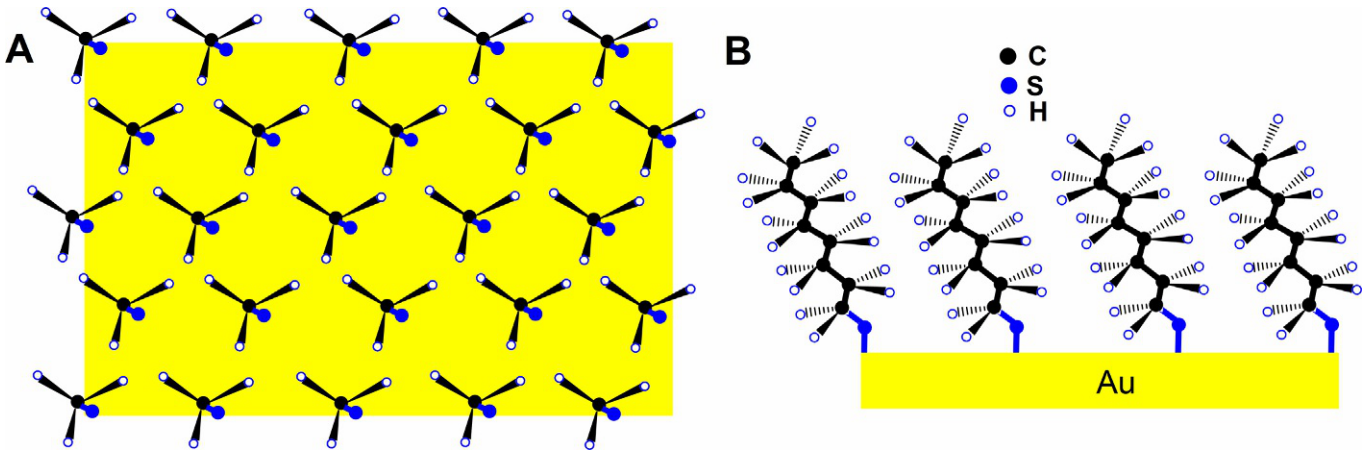


**Fig. 2** Illustration of the self-assembled monolayer absorbed on a representative gold film. Graphic illustration of top (A) and front (B) views.

bulk structure, some $Si^{4+}$ cations from tetrahedral sites are replaced by $Al^{3+}$ cations (Al/Si ratio = 1:3), resulting in a permanent negative charge, offset by some alkaline cations such as $K^{+}$. The nature and location of these ions strongly influence the properties of the mica surfaces. Besides, when muscovite is exposed to a wet environment, a thin layer of water molecules is formed on the surface, further modifying the surface properties [16].

The CLAYFF [26] force field is one of the most suitable atomistic representations to simulate muscovite surfaces in theoretical computational studies, since it was explicitly developed for muscovite systems [26]. This force field has the advantage of quantifying support-adsorbate interactions with simple arithmetic and geometric averages from Lennard-Jones parameters [27]. However, several problems arise when using this model for the support. The first one is the high computational cost when using relatively large surfaces (a typical surface area being $\sim 60 \times 60$ Å$^2$). This fact limits the studies to a few nanoseconds simulations.

A very convenient support, to consider in theoretical studies, is graphite, since it does not present active sites for forming covalent bonds with adsorbates. Graphite models have been widely used as an ultra-thin surface for the deposition of different molecules including water, lipids, proteins, ionic liquids, etc. [28, 29].

There are two common ways to use graphite as support at a low computational cost. One uses the generalized amber force field (GAFF) [28], building many graphite sheets on top of each other to stabilize the surface. The other approach involves just one or two layers of graphite and freezes all the other graphite atoms (Fig. 3). When freezing graphite atoms, only Lennard-Jones parameters are necessary to simulate the interactions with support. This approach has already been used successfully, as reported in literature [30, 31].

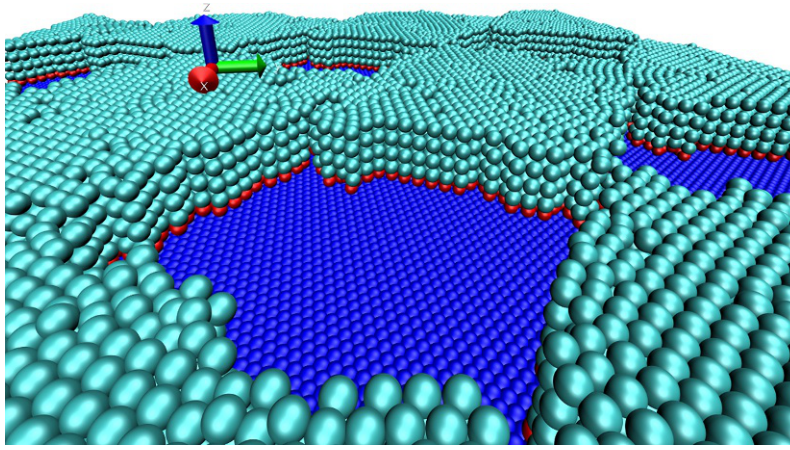


**Fig. 3** Graphene support where all surface atoms are frozen (in *blue* (grey in the print version)). This support is used to deposit the PAL cutin monomers. (For interpretation of the references to colour in this figure legend, the reader is referred to the web version of this article.)

Other support models based on different types of Lennard-Jones potentials allow the possibility to cover a greater number of properties of the given system [32]. These models were widely used in early studies of cutin monomer deposits [33]. They use the 12-3 external potential described by equation 1, where the $C_{12}$ and $C_3$ parameters must guarantee a much weaker adsorbate-support interaction than a substrate-substrate interaction; $Z$ is the atomic distance to the surface and $Z_0$ is a limit approach distance for each centre.

$$V_{(Z)} = \sum_{\text{surface}} \frac{C_{12}}{[Z - Z_0]^{12}} - \frac{C_3}{[Z - Z_0]^3} \tag{1}$$

## 2 Computational atomistic modelling

This section summarizes some general aspects related to the computational techniques that are used in this work. In particular, a brief description of classical molecular dynamics is provided, along with an outline of the main characteristics of the force fields.

### 2.1 Molecular dynamics

Molecular dynamics aims at predicting the time evolution of a set of particles subjected to a force field [34]. The temporal evolution of the particles is investigated under the principle of conservation of linear momentum. The set of differential equations arising for a system of N particles is solved using numerical methods. Therefore, it is initially necessary to define the position, velocity, and force that each particle experiences. Usually, initial positions and velocities are arbitrarily defined, and forces are computed from the potential expressed by Eq. (2).

$$F_i(r) = -\nabla V_{(r_1, \ldots, r_n)} = \frac{\partial V_{(r_1, \ldots, r_n)}}{\partial r_i} \tag{2}$$

Then, accelerations are estimated from the forces using the second Newton's law, and new positions of the particles can thus be obtained. This procedure is repeated a long time to generate a trajectory. Many algorithms are available in the literature to integrate the equations of motion, each with its advantages and disadvantages [35, 36]. The Verlet algorithms (Verlet, Verlet-Leapfrog, and Velocity-Verlet) are the most commonly used in classical molecular dynamics codes [34]. These algorithms are obtained from the Taylor series of the position functions $r(t + dt)$ and $r(t - dt)$ around time $t$, as expressed by Eqs. (3) and (4).

$$r_{(t+dt)} = r_{(t)} + v_{(t)}dt + \frac{1}{2}dt^2 a_{(t)} + \cdots \tag{3}$$

$$r_{(t-dt)} = r_{(t)} - v_{(t)}dt + \frac{1}{2}dt^2 a_{(t)} - \cdots \tag{4}$$

## 2.2 Force field in molecular dynamics

A general expression to calculate the potential energy of any system in which particles are or are not correlated is given by Eq. (5) [37]. The argon gas system is an example of not correlated particles, whereas systems made of organic molecules are examples of correlated ones.

$$V_{(r)} = \sum_i V_{1(r_i)} + \sum_i \sum_{j>i} V_{2(r_i, r_j)} + \sum_i \sum_{j>i} \sum_{k>j>i} V_{3(r_i, r_j, r_k)} + \cdots + \sum_i V_{\text{molecular}} \tag{5}$$

The first term in the sum on the right hand side represents the interaction of the system with an external potential; this is commonly used as a support model. The second term describes the interaction between any two particles. The third term corresponds to the interaction between any three particles, and so on. The $V_{\text{molecular}}$ term is the potential of a set of particles correlated with each other (for instance, organic molecules).

The $V_{2(ri,rj)}$ term is one of the most important and is usually split into two contributions: electrostatic and van der Waals interactions. The third potential term ($V_{3(ri,rj,rk)}$) is usually negligible for gas and liquid phase systems; however, it has to be considered for inorganic systems, such as crystalline metals, or amorphous systems, such as silica glass. The fourth potential term and the ones following it have tiny contribution compared to the third term, and they are generally discarded.

The total potential equation can be satisfactorily rewritten for many organic systems, by including only the $V_{1(ri)}$, $V_{2(ri,rj)}$, and $V_{\text{molecular}}$ terms. $V_{\text{molecular}}$ is, in most cases, the sum of $V_{\text{bond}}$, $V_{\text{angle}}$, and $V_{\text{dihedral}}$. Therefore, in this case, the total potential energy equation is expressed by Eq. (6); graphical representations are given in Fig. 4.

$$V_{\text{system}} = V_{\text{bond}} + V_{\text{angle}} + V_{\text{dihedral}} + V_{\text{Coulomb}} + V_{\text{van-der-Waals}} \tag{6}$$

The $V_{\text{bond}}$, $V_{\text{angle}}$, and $V_{\text{dihedral}}$ potentials can in principle be represented by any analytical function. The different ways of defining these terms delimit different types of force fields such as CHARMM [38], OPLS [39], AMBER [40], and COMPASS [41]. In these force fields, each atom in the molecules is usually represented explicitly, and for that reason, this chapter refers to computational atomistic methods.

# 3 Experimental surface characterization

This section briefly describes some experimental techniques widely used in surface characterization to obtain valuable information from self-assembled structures.

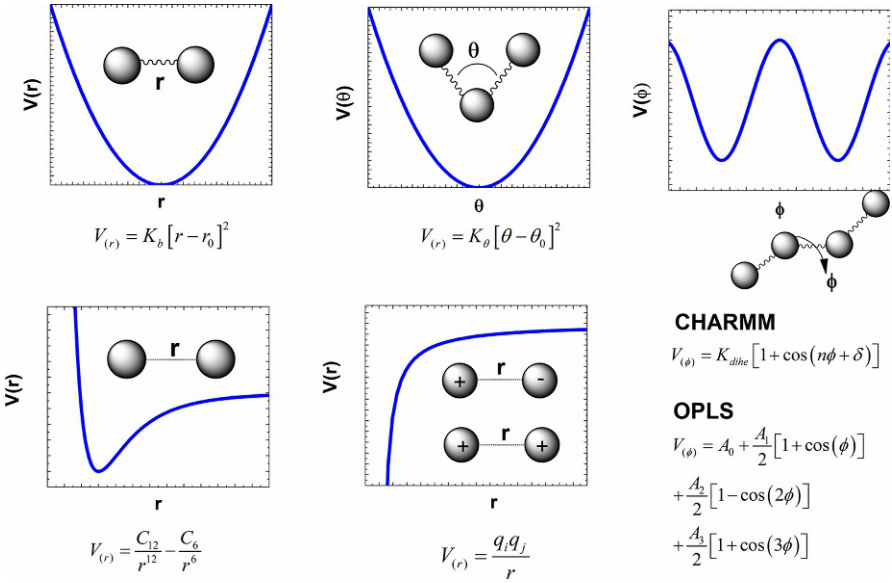


**Fig. 4** Schematic representation of the common potential functions used in classical molecular dynamics simulations. The $V_{\text{dihedral}}$ potential is displayed for the CHARMM and OPLS force fields.

## 3.1 Spontaneous self-assembly processes

The concept of spontaneous self-assembly of molecules forming a self-assembled monolayer (SAM) is intimately related to their competition for the adsorption sites [42]. Chemisorption provides the driving force of the process and conditions the robustness of the adhesion. Thus, organic molecules are chemically functionalized to ensure strong bonding with the support. Thiolates were one of the first successful systems used because of the high chemical affinity of the terminal –SH groups with most of the transition metals [43]. The concept of chemical modification of the exposed terminal side of the monolayer has also been employed to add functionality or passivate the self-assembled layer. Thus, more selective or efficient systems can be prepared for adsorption and adsorbate recognition, passivated and antifouling surfaces, and for the fabrication of more complex, compatible, and hierarchical functional multilayered systems in optoelectronics, and miniaturized devices (MEMs) [44].

However, much less attention has been paid to self-assembling processes driven by moderate chemical or electrostatic forces with the substrate, as is the case, for instance, when organic molecules or macromolecules and relatively inert substrates like graphite, silicon, and silicates are used. In these cases, the cohesive intermolecular interaction becomes comparable to the adsorption energy and constitutes an important contribution to the energy balance and the stability of the layered system.

It also has to be kept in mind that self-assembled systems are confined and well-ordered structures and, therefore, are suitable to be studied by a series of high-resolution analytical techniques and modelled by theoretical methods. The combination of such methodologies provides essential information for the design of thin polymeric coatings in terms of the chemical structure and functionalization of the monomer to be used.

## 3.2 Scanning probe microscopies

Among the analytical techniques used for the analysis of self-assembled systems on a flat support, scanning probe microscopies (SPM) (i.e., scanning tunnelling microscopy (STM) and atomic force microscopy (AFM)) have become very useful and widely used. Their success is based on their high resolution and real-space visualization of structures; also, in their versatility and capability to provide additional electric, electrostatic, mechanical, tribological, and, to a lesser extent, chemical mapping in virtually any environment (UHV, air, liquid). The full control over the probe's physical-chemical conditions and positioning allows either a passive operation as a mere sensor or an active and response sensing actuation by perturbing the sample to a controlled extent. An example of such an active operation is the so-called scanning probe lithography (SPL) by which 2D and 3D nanostructures can be created on top of a surface by the precise control of the local tip-molecule-surface interactions [45] and sets the frontier for molecular-scale manipulation.

The elucidation of the structure of the molecular packing within a self-assembled layer using atomic force microscopy (AFM) requires some degree of interaction between the scanning probe and the molecules by chemical, electrical, and magnetic of van der Waals forces. Although such interaction has been significantly reduced along with the development of instrumentation (improvements in probe fabrication, transducers, electronic control, etc.), still it may represent a perturbation high enough to be overcome by energy dissipation mechanisms within the SAM and cause a reversible/irreversible disruption of the molecular arrangement. In highly bonded SAMs, such as thiols on transition metals, the robustness of the S-M linkage resists the mechanical action of the scanning probe and molecular resolution images can be obtained, particularly from lateral force (friction) mapping. Other supports, flat enough to be compatible with the high-resolution AFM operation, such as HOPG (highly oriented pyrolytic graphite) and mica are much less chemically reactive than metals and the anchoring of molecules is weaker. Nevertheless, high-resolution images have also been obtained for silanes on mica due to the formation of robust electrostatic Si–$O^{-}$…$^{+}$Si–O– bridges. In these cases, and conditioned by the strong bonding between the substrate and the molecule head group, the alkyl skeleton is oriented mostly vertically or slightly tilted to the support plane.

However, in the case of fatty acids packing on HOPG, the maximization of the molecule-substrate interaction (as well as the intermolecular head group interplay) drives the molecule to lie flat to the substrate. Such re-orientation is clear evidence of the driving influence of the substrate on the final structure of the alkyl molecule packing in SAMs. If interest is focused on how the intermolecular interactions

condition the conformation of the molecular packing, the support can be considered as a perturbing agent and its participation must be reduced as much as possible. Keeping in mind that a substrate is necessary for the AFM analysis, this is postulated by using a quite inert flat support such as mica (muscovite). In such conditions, and using fatty amphiphilic ($C_8$–$C_{18}$) molecules such as carboxylic acids and amines, mono and multilayer stacking was observed, as well as compaction and segregation phenomena driven by functional groups within the molecule architecture. Unfortunately, the cost of using a low-interacting substrate impedes molecular resolution AFM imaging. However, this is mitigated by the obtaining of indirect additional information that allows postulating a structural model. For instance, an effective packing of linear molecules is indirectly reflected in the appearance of discrete flat islands with a well-defined height. Height values also reflect the tilting degree of the molecular axis to the substrate normal and the characterization of multilayer distributions. Additional information such as friction and adhesion mapping can be obtained in parallel to topography imaging with AFM. Both are intimately related with specific local physical-chemical interactions between the probe apex and terminal functional groups of SAMs and, consequently, provide some degree of chemical characterization of surface motifs. For instance, hydrophobic and hydrophilic terminal groups can be easily differentiated by frictional and adhesion contrast, which can allow the setting of the molecular axis orientation to the substrate.

## 4 Molecular assembling from pure monomers

In recent years, some cutin monomers in the $C_{16}$ family have been extensively investigated. Some of the research presented in this section tackles their structural and chemical behaviour when deposited on inert support. Specifically, it focuses on ALE and PAL molecules because they are representative models as active and non-active monomers for the self-assembly processes.

### *4.1 Deposition of ALE system on a flat support*

MD simulations show that the arrangement adopted by ALE molecules, when deposited on a support, depends strongly on the effective surface density ($\rho$). Four zones with different behaviours are observed (Fig. 5), and the ALE molecules have different degrees of organization in each of these zones. At high effective surface density ($\rho = \sim 5.2 \times 10^{-4}$ molecules/Å$^2$, Fig. 5, zone 1), the system exhibits self-assembly behaviour for a short time, and around 2 ns of simulation, it loses this arrangement reaching disordered configurations (Fig. 5).

The energy change involved in this process is due to the loss of the (–COOH)—(–COOH), (SOH)—(SOH), and (POH)—(POH) hydrogen bonds (Fig. 5A) and also the formation of the (–COOH)—(SOH), (–COOH)—(POH), and (POH)—(SOH) hydrogen bonds (Fig. 5B), where POH denotes a primary hydroxyl and SOH denotes a secondary hydroxyl.

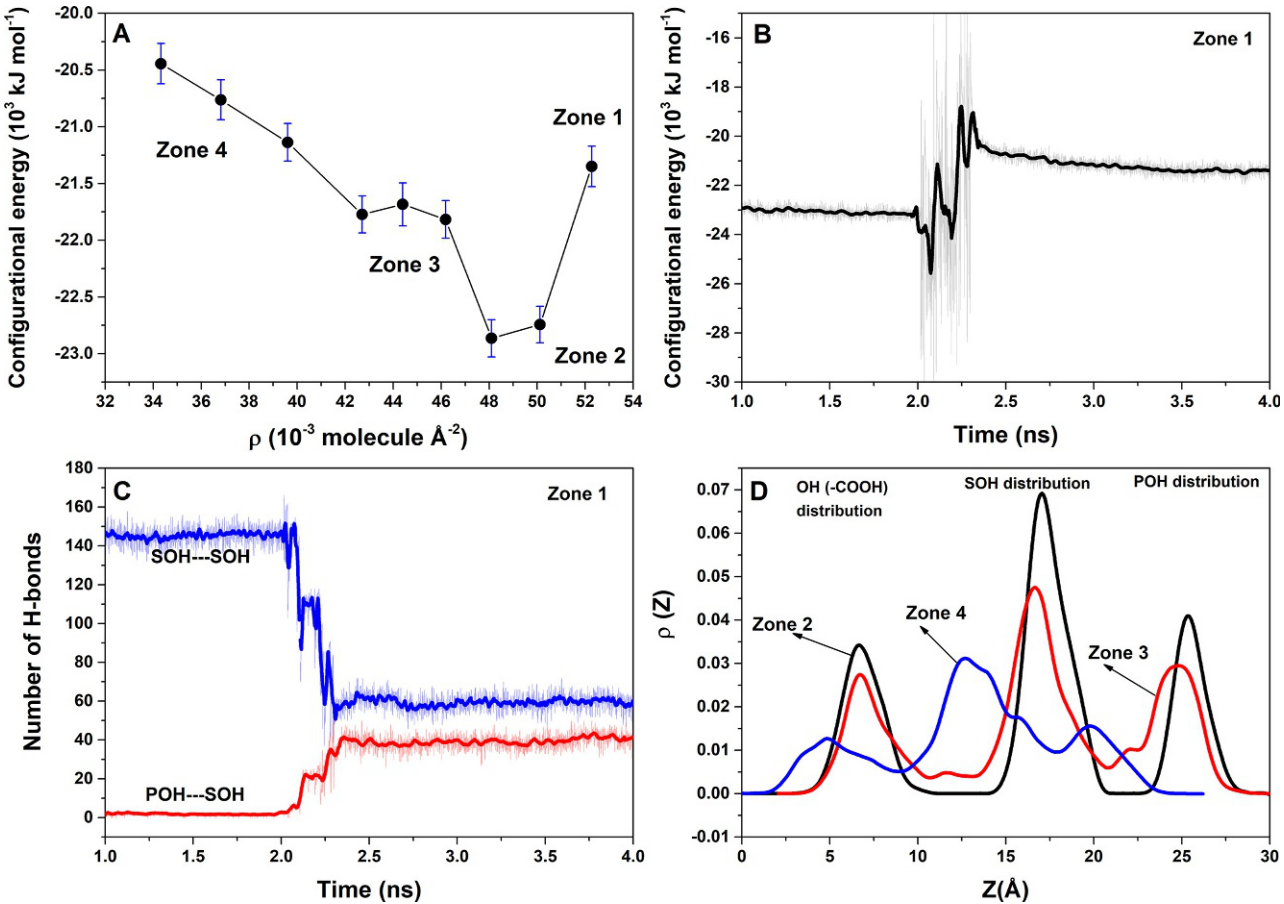


**Fig. 5** (A) The configurational energy as a function of the effective surface density ($\rho$) of pure ALE. (B) The configuration energy as a function of the simulation time of the ALE system deposited in zone 1. (C) Evolution of the number of H-bonds in the ALE system (zone 1). Hydrogen bonds in (SOH)—(SOH) and (POH)—(SOH) interactions. (D) Density profile along the *Z*-axis of the COOH, POH, and SOH groups in zones 2, 3, and 4.

At the other extreme, when deposited at low effective surface density, for example, in zone 4 ($\rho = \sim 3.4 \times 10^{-4}$ molecules/Å$^2$), the system does not have self-assembling capacity, and disorganized ALE monolayers are observed. A density profile along the $z$-direction shows that the COOH, SOH, and POH groups are indeed superimposed on each other (Fig. 5C). When ρ increases, for example, from $3.7 \times 10^{-4}$ to $3.9 \times 10^{-4}$ molecules/Å$^2$, the systems do not self-assembly either. However, it was also observed that the superposition between these groups decreases slightly, mainly between the COOH and POH groups. The SOH groups—main responsible for the organization—still cannot present a homogeneous profile distribution along the $z$-direction.

On the other hand, in the area between zone (2) and zone (3), the deposition of ALE always leads to self-assembled systems. Specifically, in zone 2, the systems achieve the highest stability. For example, for deposition with $\rho = 4.8 \times 10^{-4}$ molecules/Å$^2$, the density profile analysis shows that the COOH, POH, and SOH groups have symmetrical distribution, and they are not overlapped (Fig. 5A). For this ρ value, the maximum capacity of self-organization is achieved.

In zone 3, whatever the effective surface density, the configurational energy is similar; that is, the systems' stability stays constant (Fig. 5B). In this zone, depositing ALE leads to the formation of self-assembled systems with similar configuration stability.

## 4.2 Pure ALE and PAL systems behaviour

The MD simulations of pure ALE systems show a self-assembling behaviour with slightly inclined ALE molecules relative to the $z$-direction. As expected, the effective surface density value of $\rho = 4.8 \times 10^{-4}$ molecules/Å$^2$ (zone 2) guarantees this behaviour. Although the effective surface density study was done from MD simulations for ~2 ns, the results were confirmed for extended simulations until 40 ns, and they are presented in Fig. 6A. It is observed that the system remains self-assembled for all simulation time, and the distribution of the active groups (COOH, POH, and SOH) remains the same.

For pure PAL systems, the molecules are disorganized regardless of the effective surface density. The density profile in Fig. 6B shows this behaviour. It is observed that, for 5–10 ns of simulation, the molecules are not only oriented in different directions, but also on top of each other. This fact suggests that the COOH groups do not have sufficient capacity to form H-bonds that guarantee the self-assembly. The next section analyses this proposition.

## 4.3 Chemical reaction in ALE systems

### 4.3.1 Techniques to evidencing esterification reactions

Fatty polyhydroxy acids have been found to have the capability to self-assembly and self-esterify at ambient conditions to form nanometre-size particles named cutinsomes [19]. Such nanoparticles have been detected *in planta* [18], and they can further

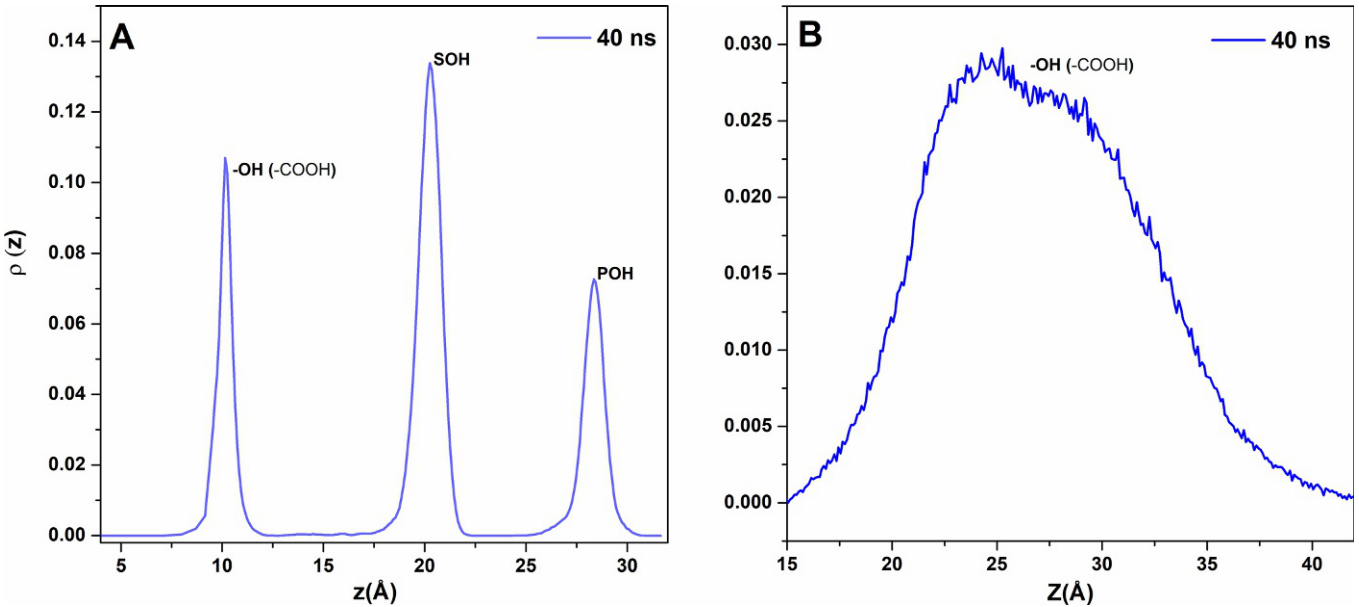


**Fig. 6** Mass density profiles along the z-axis of the active groups: (A) COOH, POH, and SOH, in pure ALE system, and (B) COOH, in pure PAL system.

aggregate and spontaneously polymerize at standard environmental conditions to form a continuous polyester layer, thus providing a plausible mechanism for in vivo cutin biosynthesis [46, 47]. Such a hypothesis is gaining recognition since analogous nanometre-size structures have also been recently detected in the elucidation of the molecular architecture of suberin [48].

The importance of these studies lies in the transference of this seminal knowledge to the design and manufacturing of biodegradable biomimetic materials with potential applications as protective films for food and cosmetics packaging [49–52]. Therefore, investigating other properties, in addition to the structural ones such as the possibility of esterification reaction (ER), is of great importance.

The first ER studies by attenuated total reflection Fourier transform infrared (ATR-FT-IR) spectroscopy, X-ray photoelectron spectroscopy (XPS) and molecular dynamics (MD) techniques in self-assembled (SABs) systems of ALE bilayers showed that the esterification reaction could occur as a consequence of the self-assembling (SA) [33].

The next subsections present the latest advances in ER in pure ALE systems, when deposited on an inert flat support. MD simulations reveal two possible ways to favour an ER, namely, route 1 (R1), involving interactions between COOH and POH groups, and route 2 (R2), involving interactions between COOH and SOH groups (Fig. 7). Possible ERs in pure ALE systems are explored in the next subsection, with reference to these ways.

### 4.3.2 Esterification reaction in organized ALE bilayer

In bilayers systems, the only way to favour an ER is through route R1, that is when COOH and POH groups interact. The interaction between these groups was analysed using radial distribution functions (RDF) for C—O and H—O distances. The $g_{(C—O)}$ ($\delta_1$) curve presents two peaks at 3.2 and 3.7 Å, whereas the $g_{(H—O)}$ ($\delta_2$) shows three peaks at 1.8, 3.0, and 3.8 Å.

Analysing these peaks and relating them to a possible ER is not trivial. By taking advantage of the fact that $\delta_1$ and $\delta_2$ would be correlated if an ER were given, combined distribution functions (CDF) were used to poll zones where an ER can occur. Using the TRAVIS code [ [53]], it is possible to do all these analyses, and the results are shown in Fig. 7. These results show the presence of three predominant zones: zone 1, with $1.6 < \delta_1 < 2.5$ Å and $3.5 < \delta_2 < 4.0$ Å; zone 2, with $2.5 < \delta_1 < 3.3$ Å and $3.0 < \delta_2 < 3.8$ Å; and zone 3, with $3.5 < \delta_1 < 4.5$ Å and $3.4 < \delta_2 < 4.1$ Å. Among these zones, COOH and POH groups get an adequate configuration to favour an ER only in zone 1, as peaks at $\delta_1 = 3.7$ Å and $\delta_2 = 1.8$ Å suggest that an ER could occur. For this reason, the presence of these peaks is the only one monitored in the study of the next systems.

Furthermore, when comparing the relative intensity of all zones, it is clear that the zone that favours an ER (zone 1) is rarely visited. This suggests that organized bilayers of ALE systems would have difficulty in initiating the reaction since the system remains for most of the time in zones 2 and 3.

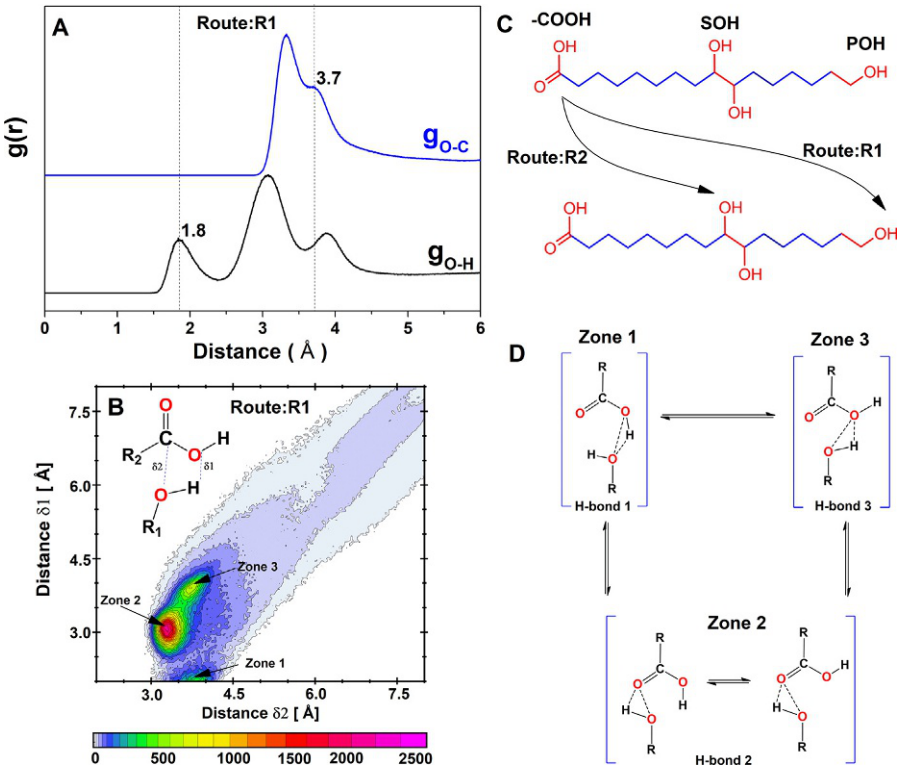


**Fig. 7** (A) Radial distribution functions (RDF) for O—C ($g_{OC}$) and O—H ($g_{OH}$) distances with characteristic peaks at 3.7 and 1.8 Å corresponding to nucleophilic attack ($\delta_2$) and water formation ($\delta_1$) in R1 route for bilayer ALE system. (B) Combined distribution function (CDF) with channels being $\delta_1$ and $\delta_2$ distances for bilayers L3 in ALE system. (C) Interacting groups in esterification reaction (ER): COOH and POH groups in route 1 (R1), and COOH and SOH groups in route 2 (R2). (D) Molecular configurations with COOH and OH groups interacting in a self-assembled bilayer.

The configurational arrangements that exist in those three zones were analysed and can be schematically summarized as shown in Fig. 7. In zone 1, there is a configuration possibly stabilized by H-bond interactions formed by the POH group and the protonated oxygen of the CO**O**H group (H-bond 1, HB1). If this type of H-bond exists, its presence will guarantee an initial configuration needed to favour an ER.

In zone 2, two different configurations were found that are also possibly stabilized by H-bond interactions. In this zone, the POH group interacts with the oxygen in the carbonyl of C**O**OH (H-bond 2, HB2). This type of H-bond prevents an ER from occurring, since it would not be possible to get a fitting initial configuration.

Similarly, the main configuration in zone 3 may also be stabilized by H-bond interactions, in which the hydroxyl of the COOH group interacts with the oxygen of the POH (H-bond 3, HB3). This configuration also prevents an ER from occurring.

All these results show that two requirements need to be met for an ER to be favoured: the hydrogen of the COOH group has to form a dihedral angle of 180 degree respect to the CO, and there must be H-bond interactions of type 1 (HB1). The presence of the three types of H-bonds (HB1, HB2, and HB3) was confirmed by combined distribution function (CDF): radial and angular distribution functions (RDF and ADF) were used to verify the presence of H-bond ($r_{o\text{-}o}$ and $\alpha$), and the results are presented in Fig. 8.

An analysis of all possible H-bonds shows that all zones are actually stabilized by H-bond interactions ($r_{o\text{-}o} < \sim 3.0$ Å and $\alpha < \sim 20°$). It was also confirmed that the local minimum in zone 1 is the least stable because of having the smallest number of H-bonds (HB2/HB1 and HB3/HB1 ratios ~2.5 and ~4.3, respectively). This result is consistent with the observation that the local minimum that favours an ER (zone 1) is the least visited and is not the most stable region.

### 4.3.3 Esterification reaction in disorganized ALE monolayer

In disorganized ALE monolayer systems, an ER could occur through both routes (R1 and R2). On analysing the interactions in the two reaction routes, it is observed that there are peaks at $\delta_1 = 3.7$ Å and $\delta_2 = 1.8$ Å, related precisely to zone 1 (where an ER could occur, Fig. 9); the presence of the peak at d(C—O) = 3.7 Å ensures a required approximation distance favourable to a nucleophilic attack. Also, the peak at d(O—H) = 1.8 Å indicates a propitious distance for the formation of the water molecule. Furthermore, it is observed that the R2 route is the least favoured even though the groups involved (COOH and SOH) are closer, but their interactions are less effective to ER. Since route R1 predominates, this could lead to the formation of more disorganized monolayers than it would be if the route R2 were the most favoured.

## 5 Structural processes of binary mixtures

Once the main characteristics of processes involving pure monomers of ALE and PAL have been analysed, the next step is studying mixtures of both.

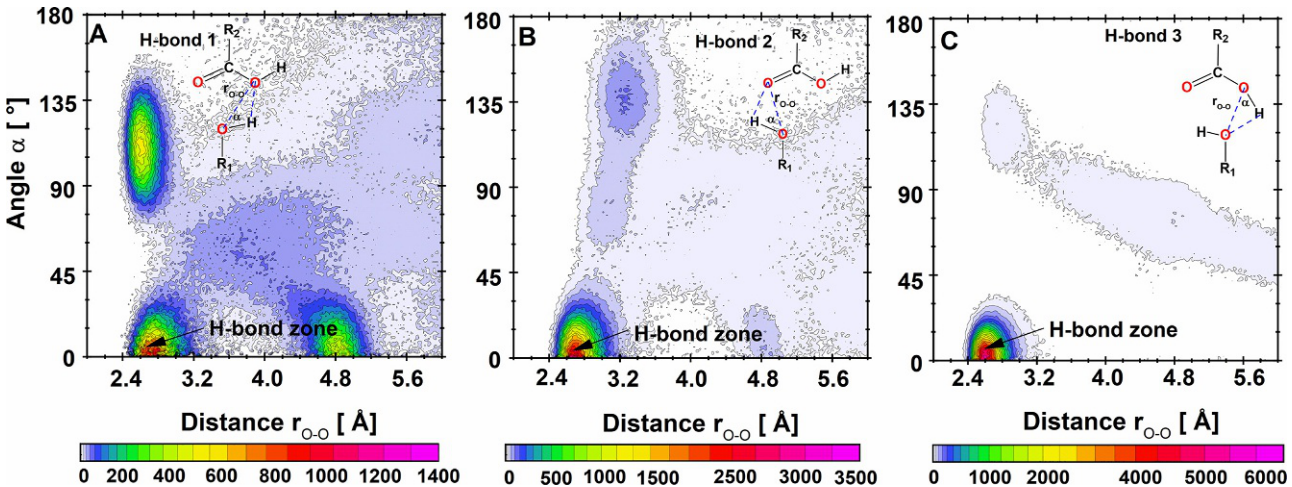


**Fig. 8** Combined distribution functions (CDF) with one channel being a distance $r_{o-o}$ and the other being an α angle. (A) For H-bond 1, (B) for H-bond 2, and (C) for H-bond 3, in bilayer ALE system.

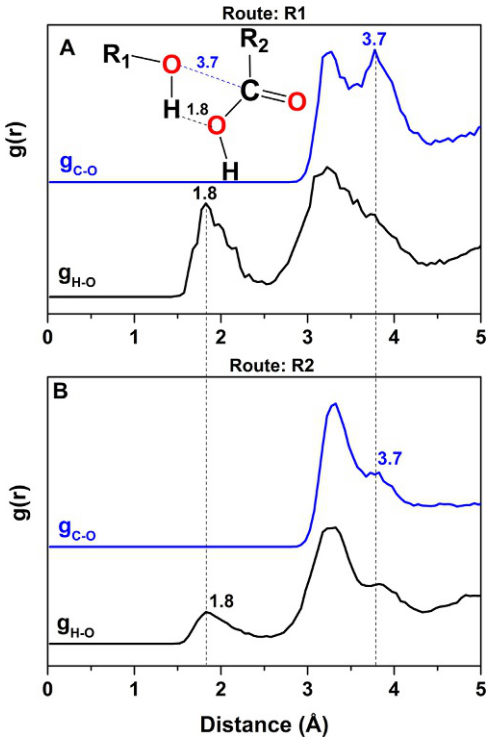


**Fig. 9** Radial distribution function (RDF) of the (A) COOH and POH groups, route 1 and (B) COOH and SOH groups, route 2, in unorganized monolayer ALE system.

## 5.1 ALE and PAL mixtures

As shown in the previous sections, specific intermolecular interactions determine the final arrangement of packed alkyl molecules. Such molecular arrangement drives the layer termination and therefore conditions its interaction with the environment. Chemical reactivity and hydrophobicity or hydrophilicity of exposed groups are essential to define properties such as friction, adhesion, and chemical inertness of layers formed by self-assembly. In the field of polymer science, the tailoring of the molecule functionalization and the study of self-assembling processes help gather crucial information on aspects such as the wettability on a surface and nanoparticle capability formation and the coalescence of such entities. All of them are critical factors in designing polymer coatings. On the other hand, there are macromolecular synthetic and bio-synthetic routes involving the formation of nanoparticles and their consequent aggregation to obtain bulk polymers. The modification of the structure of such aggregates via inter and intramolecular manipulation of the monomers is a tool to modify the final properties of the resulting material. The study of fundamental issues such as the compatibility/non-compatibility (segregations) between functional groups within the monomer skeleton using the proposed methodology is a preliminary step to outline a synthesis route. In the case of the preparation of polyhydroxyesters resembling natural cutin, the process necessarily starts from the monomer mixture obtained from

cutin depolymerization. This mixture is composed of fatty and mono and polyhydroxy fatty acids, and an economically viable process cannot include monomer separation stages. Thus, mixtures of palmitic (PAL) and aleuritic (ALE) acids were selected, respectively, representing the non-hydroxylated and the most hydroxylated monomers present in natural cutin. The next subsection describes the structural behaviour of mixtures of ALE and PAL monomers, when deposited on a flat support, for high (75% ALE and 25% PAL) and low (25% ALE and 75% PAL) ALE compositions.

## 5.2 ALE and PAL mixture stability for 75% and 25% compositions

The structural stability of the mixtures is analysed using the configurational energy. Various types of homogeneous and segregated systems were analysed to obtain statistical behaviour. The results for both 75:25 and 25:75 (ALE:PAL) compositions are shown in Fig. 10A and B.

For 75:25, all segregated systems are more stable than dispersed systems. This observation is evident by comparing the average configuration energies values: $-2.2 \times 10^2$ and $-2.1 \times 10^2$ kJ/mol for segregated and dispersed systems, respectively. Therefore, it would be expected that, for systems with high ALE proportion, segregation processes might be favoured. Also, when analysing each system separately, it is observed that all segregated systems are more stable than any dispersed system, indicating that the formation of segregated systems is markedly favoured.

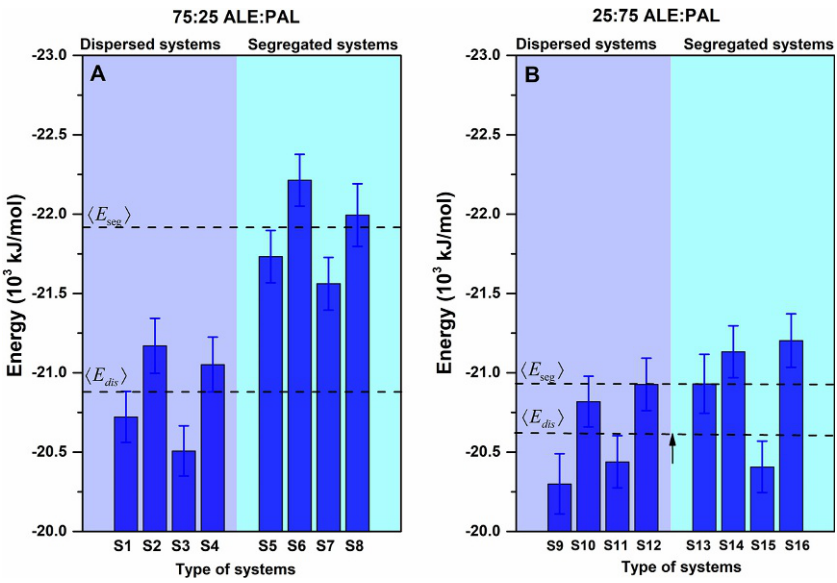


**Fig. 10** Configurational energy for systems with compositions of (A) 75:25 and (B) 25:75 ALE:PAL. For both, different types of segregated and dispersed systems were built to obtain their average behaviour.

However, there are dispersed and segregated systems with small differences in configurational energy, suggesting a possible coexistence of both systems.

For 25:75 (ALE:PAL) composition, the mean configurational energy difference between the segregated and dispersed systems decreases to $-4.5 \times 10^2$ kJ/mol (Fig. 10B), making the appearance of dispersed systems feasible. In fact, the analysis shows that, unlike the previous case, there are dispersed systems more stable than segregated ones.

Therefore, based on the configurational energy, it can be concluded that systems with a higher amount of ALE (75:25) favour the formation of segregated phases. In contrast, systems with low ALE proportion (25:75) lead to the coexistence of segregated and dispersed phases.

## 5.3 Structural behaviour of systems with 75% ALE presence

For systems with 75:25 ALE:PAL composition, the tilt angle distributions relative to *z*-axis for ALE and PAL molecules show different behaviours. The ALE molecules present sharp mono-nodal distributions with a tilt angle between 0 and 40 degrees and peaked at 17 degree, resulting in quasi-vertical monolayers. It is also observed that the organization, verticality, and compactness of ALE molecules are enhanced in the most stable systems (segregated systems). These results indicate that systems with a high ALE proportion maintain their capacity to form ordered self-assembled systems. The height distribution profile obtained from AFM images for ALE rich (ALE:PAL) mixtures confirms the quasi-vertical packing of ALE molecules into monolayers.

Regarding PAL molecules, they are not as disorganized in segregated systems as pure PAL SAMs (Fig. 11A), due to the restriction that ALE molecules impose, mainly through the interactions between COOH groups. However, it is expected that PAL molecules that do not interact with ALE molecules tend to behave similarly to pure PAL, which has a characteristic behaviour for non-midchain functionalized amphiphilic alkyl molecules. Configurational energy values indicate that segregated islands are the most viable situation and, in fact, isolated PAL moieties ~9.0 Å high were detected by AFM [54].

## 5.4 Structural behaviour of systems with 25% ALE presence

Configurational energy calculations have shown that the 25:75 ALE:PAL system is less prone to segregation than 75:25 ALE:PAL. Simulations have also shown that the behaviour of the tilt-angle distributions of ALE and PAL are reversed in the two systems (Fig. 11B). Generally, ALE molecules are more tilted and disorganized in the 25:75 mixture than in the 75:25 one, while PAL molecules are more vertically packed. This behaviour shows that the presence of small amounts of ALE in PAL systems prevents PAL molecules from completely disorganizing and even induces locally organized PAL patches. As a result, more PAL units can be deposited in the same surface area. Also, the experimental results on surface coverage data show that the presence of ALE molecules favours PAL adsorption [54]. Therefore, it is

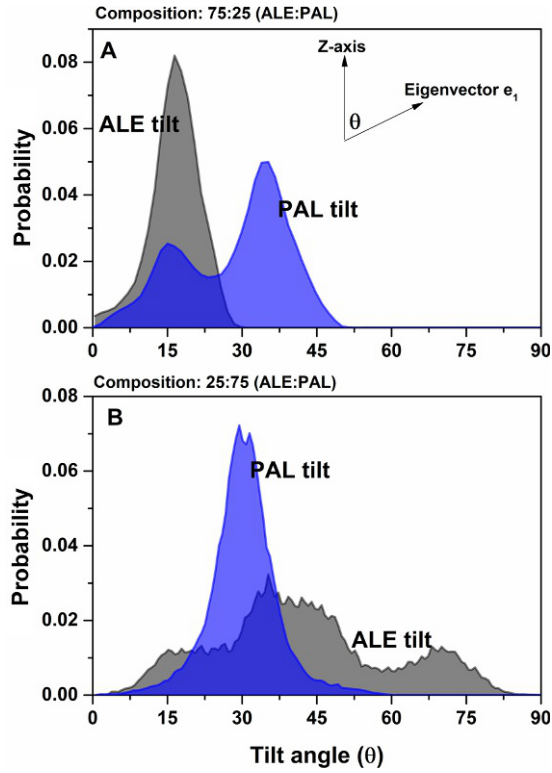


**Fig. 11** Distribution of tilt-angle formed between $e_1$ eigenvector and $z$-axial for systems with (A) 75:25 and (B) 25:75 ALE:PAL compositions (ALE and PAL in *black* and *blue* (grey in the print version), respectively). (For interpretation of the references to colour in this figure legend, the reader is referred to the web version of this article.)

presumed that in dispersed systems with low ALE proportion (25:75, ALE:PAL), some ALE molecules act as anchorage points, reinforcing lateral interactions within the SAM structure. The next section discusses the role of active groups (COOH, POH, and SOH) and how they define the stability, compactness, and degree of inclination of molecules.

## 5.5 Hydrogen bonds interactions in binary ALE:PAL mixtures

The role of H-bonds in the structural arrangement of segregated and dispersed systems is examined. For 75:25, the number of H-bonds involving POH and SOH groups is higher in segregated systems than in dispersed systems, and the number of H-bonds with COOH groups is the same in all systems (Fig. 12). Therefore, segregated systems are more stable, possibly due to the H-bonds formed between POH and SOH groups.

The number of H-bonds formed by active groups always follows the ordering SOH > POH ≫ COOH. Therefore, the SOH groups are the main responsible for building self-assembled systems. On the contrary, the COOH groups have a minor ability to form H-bonds, and consequently, they have little control over the packing

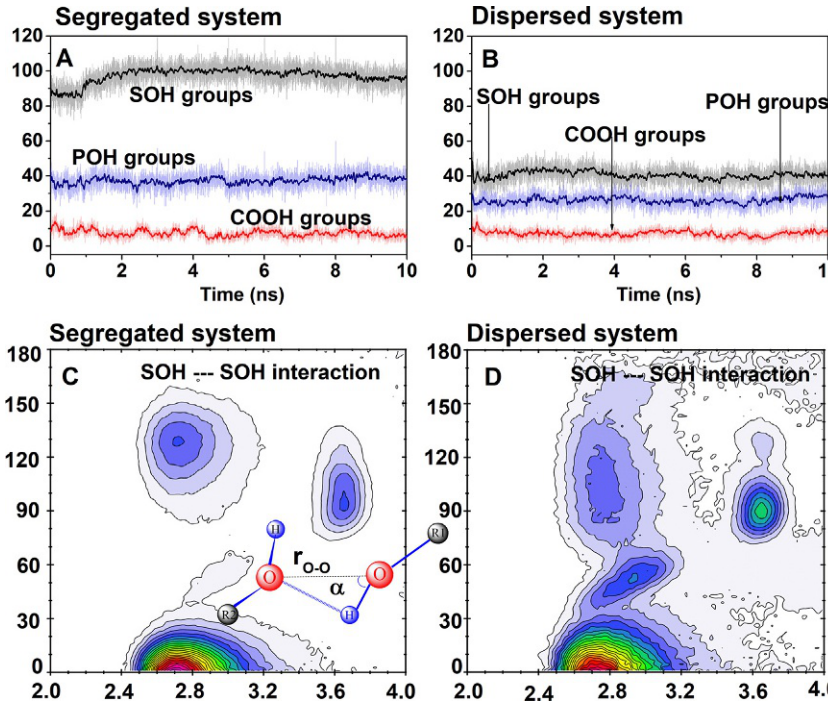


**Fig. 12** Time evolution of number of H-bonds between COOH, POH and SOH groups, for systems with 75:25 (A and B) and combined distribution functions (CDF) with two channels: $r_{o\text{-}o}$ distance and α angle (C and D).

process. This fact confirms that pure PAL systems (Fig. 6B) do not lead to organized systems. The POH groups have intermediate capacity to form H-bonds when compared to SOH groups, and, therefore, they have limited control in the organization process.

Although all the systems have the same number of SOH groups, the segregated and dispersed systems present different amounts of H-bonds. To analyse the reason for this difference, combined distribution functions (CDF) were used to monitor the variables that define an H-bond. In particular, radial and angular distribution functions (RDF and ADF) were used to monitor the $r_{0\text{–}0}$ distance and $\alpha$ angle, respectively (Fig. 12C and D). It was observed that in the segregated system, the zone that favours the formation of H-bonds ($r_{o\text{-}o} = 2.4\text{–}3.2$ Å and $\alpha = 0.0\text{–}30.0$ degrees) is dominant. It has a relative intensity of 1.42 times higher than the dispersed system. In addition, in the dispersed system, the $r_{o\text{-}o}$ and $\alpha$ parameters define zones that have no relation to an H-bond zone, mainly those zones comprising $r_{o\text{-}o} = 2.4\text{–}3.2$ Å, $\alpha = 30.0\text{–}180.0$ degrees and $r_{o\text{-}o} = 3.5\text{–}3.8$ Å, $\alpha = 70.0\text{–}150.0$ degrees (Fig. 12C). By contrast, in the segregated system, the $r_{o\text{-}o}$ and $\alpha$ parameters have values concentrated in the zone that favours the H-bond, making this system the most stable (Fig. 12D).

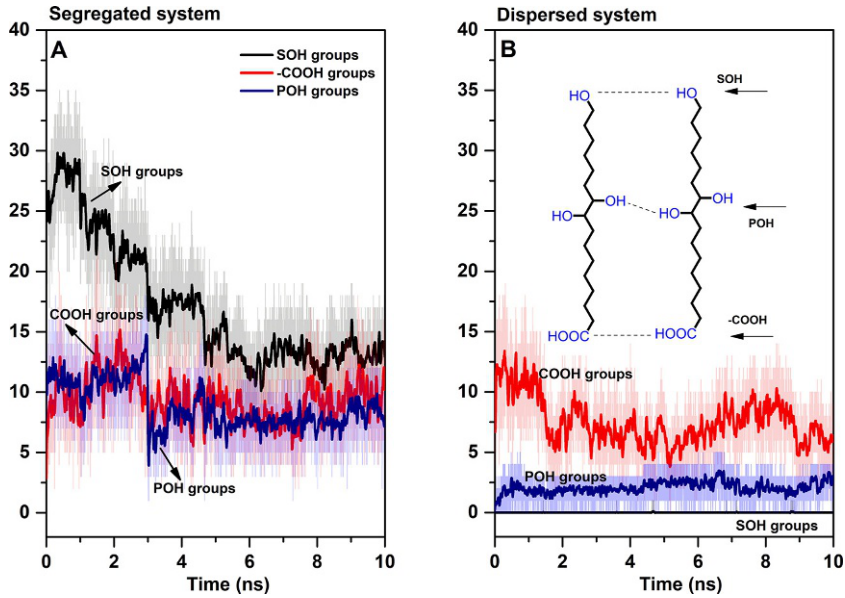


**Fig. 13** Time evolution of the number of hydrogen bonds between COOH, POH, and SOH groups, for a segregated (A) and a dispersed (B) systems with 25:75 ALE:PAL composition.

For 25:75 composition, the behaviour of the active groups is different for each system type. In the dispersed system (Fig. 13A), the COOH group has the highest number of H-bonds, and there is no H-bond formation between SOH groups. Therefore, the POH and SOH groups have less influence on stability than the COOH groups. Consistently with the previous results from density profiles, these results indicate that the ALE molecules are not organized. Also, the predominance of the H-bond between the COOH groups suggests that ALE molecules are somewhat anchored at their base. For the segregated system (Fig. 13B), the SOH groups form a higher number of H-bonds; that is, they are the dominant groups. However, the predominance of SOH groups decreases considerably in the first 5 ns of simulation; after that, all groups have practically the same prevalence. Consequently, it is expected that the ALE molecules are a little more organized in segregated systems than in the dispersed systems.

## 5.6 Segregated and dispersed systems and their coexistence

It was shown in the previous sections that the coexistence between segregated and dispersed systems is favoured for low ALE concentrations. This section further analyses this behaviour for systems with different ALE:PAL concentrations. Specifically, 18 segregated and 18 dispersed systems were investigated. Since each system contains a total of 100 molecules (ALE + PAL), each system contains a different number of atoms. Therefore, a parameter $R$ is defined (Eq. 7) to make the calculated energies comparable in terms of system stability.

$$R = \frac{-E_{\text{conf}}}{N_{\text{ALE}}E_{\text{ALE}} + N_{\text{PAL}}E_{\text{PAL}}} \tag{7}$$

where $E_{\text{conf}}$ is the total configurational energy, $E_{\text{ALE}}$ and $E_{\text{PAL}}$ are the configurational energies of an isolated ALE and PAL molecule, respectively, and $N_{\text{ALE}}$ and $N_{\text{PAL}}$, respectively, represent the numbers of ALE and PAL molecules in each system. The results of this analysis are shown in Fig. 14.

As expected, segregated systems are more stable than dispersed systems, and it becomes evident that this behaviour is extended for any ALE:PAL composition. The effect of adding PAL molecules to ALE systems can be observed for concentrations less than 75:25 (Fig. 14). This means that there is a range (ALE:PAL, 75:25–100:0) where the self-assembling behaviour of ALE systems is maintained without being drastically affected by the introduction of PAL molecules.

## 6 Final remarks

This chapter has focused on a kind of green materials with physical and chemical properties very similar to plant cutin. These materials constitute the basis for a family of bioplastics with green characteristics such as non-toxicity and biodegradability, and also with daily applications such as for thin films for better preservation of foods. The

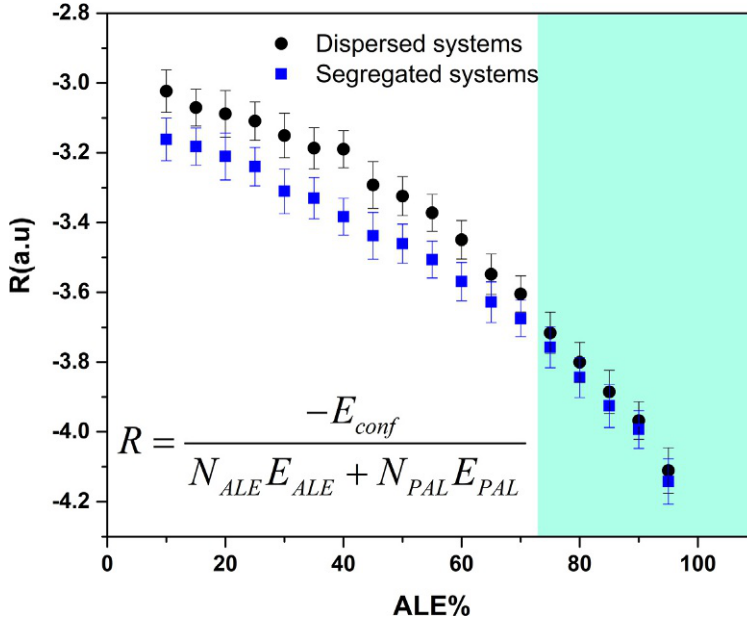


**Fig. 14** System stability computed from the R parameter as a function of ALE:PAL composition.

fact that they can be fabricated easily from abundant and available sources makes them very attractive, although there are still problems related to the physical chemical processes involved. As seen along this chapter, the use of computational atomistic techniques has become a crucial strategy in understanding some of these issues at atomic level. Specifically, the computational simulations have elucidated the causes for observed segregation processes, and also showed the tolerance of viable compositions in mixtures of two representative molecules. The same techniques can be extended to other mixtures, contributing to the efficient design of novel green materials.

## 7 Conclusions

The deposition of ALE and PAL cutin monomers on inert support shows unusual structural behaviours. MD simulations indicate that ALE deposition leads to the formation of well-behaved self-assembled monolayers where the SOH groups play a central role in the self-assembling mechanism because they control the formation of hydrogen bonding networks guarantying system stability. On the contrary, pure PAL deposition leads to disorganized systems.

In the case of mixtures, segregation processes are favoured at high ALE concentration mixtures in agreement with the experimental pieces of evidence. Meanwhile, for compositions with low ALE concentration, coexistence between segregated and dispersed systems is promoted.

Despite the limitations of classical MD simulations to study chemical reactions, valuable parameters were revealed to infer possible ER routes that occur when ALE molecules are deposited on a support.

The loss of ability for self-assembling of these systems leads to favouring esterification reactions, and as the disorder increases, the number of esterification routes also increases. For example, in pure ALE systems, it is observed that SAMs cannot form ER. However, when monolayers are disorganized, the R1 and R2 routes are favoured. For bilayer pure ALE systems, where the system is well organized, only the R1 route is favoured due to interactions between COOH from the upper layer with the POH in the lower layer.

This work proves how the combination of experimental and atomistic computational techniques to study model systems allows a valuable understanding of the fundamental physical chemical processes of complex processes. It was demonstrated that ALE and PAL's choice as representative molecules aids in explaining phenomena occurring in the early stages of procutin formation such as self-assembling, disordering, or segregation processes. This crucial information is precious for the design of ultra-thin layers and coatings with green characteristics, demonstrating the relevance of the computational chemistry in the development of novel green materials.

## Acknowledgements

This work was funded in part by Fundação de Amparo à Pesquisa do Estado de São Paulo–FAPESP (2013/07296-2; 2016/23891-6; 2017/26105-4). This work used computational

resources of the 'Centro Nacional de Processamento de Alto Desempenho em São Paulo' (CENAPAD-SP), 'Centro de Computação John David Rogers' (CCJDR-UNICAMP), and the CENAPAD-RJ (SDumont). This work was funded by National Council for the Improvement of Higher Education (CAPES).

## References

[1] A.I.K.S. Rupp, P. Gruber, Biomimetic groundwork for thermal exchange structures inspired by plant leaf design, Biomimetics 4 (4) (2019) 75.
[2] O. Speck, T. Speck, An overview of bioinspired and biomimetic self-repairing materials, Biomimetics 4 (1) (2019) 26.
[3] G.C.D. Silva, et al., Estudo da substituição do nylon por compósito de polipropileno com fibra de vidro, Matéria (Rio de Janeiro) (2019) 24.
[4] R. Mohee, et al., Biodegradability of biodegradable/degradable plastic materials under aerobic and anaerobic conditions, Waste Manag. 28 (9) (2008) 1624–1629.
[5] W.D. Luzier, Materials derived from biomass/biodegradable materials, Proc. Natl. Acad. Sci. 89 (3) (1992) 839–842.
[6] S. Hauff, et al., Determination of hydroxylated fatty acids from the biopolymer of tomato cutin and their fate during incubation in soil, Phytochem. Anal. 21 (6) (2010) 582–589.
[7] M. Frusic-Zlotkin, et al., The interaction of pemphigus autoimmunoglobulins with epidermal cells: activation of the Fas apoptotic pathway and the use of caspase activity for pathogenicity tests of pemphigus patients, Ann. N. Y. Acad. Sci. 1050 (1) (2005) 371–379.
[8] K. Sugita, et al., Innate immunity mediated by epidermal keratinocytes promotes acquired immunity involving Langerhans cells and T cells in the skin, Clin. Exp. Immunol. 147 (1) (2007) 176–183.
[9] T.A. Luger, et al., Interleukin-6 is produced by epidermal cells and plays an important role in the activation of human T-lymphocytes and natural killer cells, Ann. N. Y. Acad. Sci. 557 (1) (1989) 405–414.
[10] C. Nawrath, The biopolymers cutin and suberin, Arabidopsis Book 1 (2002) e0021.
[11] E.G. Funhoff, et al., Hydroxylation and epoxidation reactions catalyzed by CYP153 enzymes, Enzyme Microb. Technol. 40 (4) (2007) 806–812.
[12] B. Chandra, K.K. Singh, S.S. Gupta, Selective photocatalytic hydroxylation and epoxidation reactions by an iron complex using water as the oxygen source, Chem. Sci. 8 (11) (2017) 7545–7551.
[13] M. Pollard, et al., Building lipid barriers: biosynthesis of cutin and suberin, Trends Plant Sci. 13 (5) (2008) 236–246.
[14] N. Tijet, et al., Functional expression in yeast and characterization of a clofibrate-inducible plant cytochrome P-450 (CYP94A1) involved in cutin monomers synthesis, Biochem. J. 332 (2) (1998) 583–589.
[15] J.-P. Douliez, et al., Glycerol derivatives of cutin and suberin monomers: synthesis and self-assembly, Biomacromolecules 6 (1) (2005) 30–34.
[16] J. Benítez, et al., Self-Assembly and Polymerization of Natural Occurring Fatty Acids, Advances in Materials Science Research, vol. 6, Nova Science Publishers, Inc, 2011, pp. 181–212.
[17] J.A. Heredia-Guerrero, et al., Aleuritic (9,10,16-trihydroxypalmitic) acid self-assembly on mica, Phys. Chem. Chem. Phys. 12 (35) (2010) 10423–10428.
[18] E. Domínguez, et al., Self-assembly of supramolecular lipid nanoparticles in the formation of plant biopolyester cutin, Mol. Biosyst. 6 (6) (2010) 948–950.
[19] J. Heredia-Guerrero, et al., Structure and support induced structure disruption of soft nanoparticles obtained from hydroxylated fatty acids, Soft Matter 7 (2011) 4357–4363.

[20] J.J. Benítez, J.A. Heredia-Guerrero, A. Heredia, Self-assembly of carboxylic acids and hydroxyl derivatives on mica. A qualitative AFM study, J. Phys. Chem. C 111 (26) (2007) 9465–9470.
[21] A. Mendes, et al., Self-assembly in nature: Using the principles of nature to create complex nanobiomaterials, Wiley Interdiscip. Rev. Nanomed. Nanobiotechnol. (2013).
[22] L. Srisombat, A.C. Jamison, T.R. Lee, Stability: a key issue for self-assembled monolayers on gold as thin-film coatings and nanoparticle protectants, Colloids Surf. A Physicochem. Eng. Asp. 390 (1) (2011) 1–19.
[23] G.M. Whitesides, Self-assembling materials, Sci. Am. 273 (3) (1995) 146–149.
[24] A. Mata, et al., Micropatterning of bioactive self-assembling gels, Soft Matter 5 (6) (2009) 1228–1236.
[25] M.F. Brigatti, P. Frigieri, L. Poppi, Crystal chemistry of Mg-, Fe-bearing muscovites-2M 1, Am. Mineral. 83 (7–8) (1998) 775–785.
[26] R.T. Cygan, J.-J. Liang, A.G. Kalinichev, Molecular models of hydroxide, oxyhydroxide, and clay phases and the development of a general force field, J. Phys. Chem. B 108 (4) (2004) 1255–1266.
[27] A. Abramov, S. Iglauer, Application of the CLAYFF and the DREIDING force fields for modeling of alkylated quartz surfaces, Langmuir 35 (17) (2019) 5746–5752.
[28] G. Shi, et al., Ion enrichment on the hydrophobic carbon-based surface in aqueous salt solutions due to cation-π interactions, Sci. Rep. 3 (1) (2013) 3436.
[29] Y. Yokota, et al., Structural and dynamic properties of 1-butyl-3-methylimidazolium bis(trifluoromethanesulfonyl)imide/mica and graphite interfaces revealed by molecular dynamics simulation, Phys. Chem. Chem. Phys. 20 (9) (2018) 6668–6676.
[30] M. Pykal, et al., Modelling of graphene functionalization, Phys. Chem. Chem. Phys. 18 (9) (2016) 6351–6372.
[31] S. Medina, et al., Monolayer arrangement of fatty hydroxystearic acids on graphite: influence of hydroxyl groups, Thin Solid Films 539 (2013) 194–200.
[32] J. Hautman, M.L. Klein, Simulation of a monolayer of alkyl thiol chains, J. Chem. Phys. 91 (8) (1989) 4994–5001.
[33] J.A. Heredia-Guerrero, et al., Chemical reactions in 2D: self-assembly and self-esterification of 9(10),16-dihydroxypalmitic acid on mica surface, Langmuir 25 (12) (2009) 6869–6874.
[34] C. Scheres, Métodos Computacionais da Física, 2005 ed, ed. ISBN:85-88325-35-7, vol. 1, 2005, p. 284.
[35] A.M. Namba, V.B.d. Silva, C.H.T.P.d. Silva, Dinâmica molecular: teoria e aplicações em planejamento de fármacos, Ecletica Quim. 33 (2008) 13–24.
[36] G.E. Norman, V.Y. Podlipchuk, A.A. Valuev, Equations of motion and energy conservation in molecular dynamics, Mol. Simul. 9 (6) (1993) 417–424.
[37] M.P. Allen, D.J. Tildesley, Computer Simulation of Liquids, OUP Oxford, 2017.
[38] K. Vanommeslaeghe, et al., CHARMM general force field: a force field for drug-like molecules compatible with the CHARMM all-atom additive biological force fields, J. Comput. Chem. 31 (4) (2010) 671–690.
[39] W.L. Jorgensen, D.S. Maxwell, J. Tirado-Rives, Development and testing of the OPLS all-atom force field on conformational energetics and properties of organic liquids, J. Am. Chem. Soc. 118 (45) (1996) 11225–11236.
[40] A. Nikitin, Y. Milchevskiy, A. Lyubartsev, A new AMBER-compatible force field parameter set for alkanes, J. Mol. Model. 20 (2014) 2143.
[41] H. Sun, P. Ren, J.R. Fried, The COMPASS force field: parameterization and validation for phosphazenes, Comput. Theor. Polym. Sci. 8 (1) (1998) 229–246.

[42] A. Ulman, An Introduction to Ultrathin Organic Films: From Langmuir Blodgett to Self-Assembly, Academic Press, London, 1991.
[43] R.G. Nuzzo, D.L. Allara, Adsorption of bifunctional organic disulfides on gold surfaces, J. Am. Chem. Soc. 105 (13) (1983) 4481–4483.
[44] A. Ulman, Formation and structure of self-assembled monolayers, Chem. Rev. 96 (4) (1996) 1533–1554.
[45] G. Yang, J. Garno, G.Y. Liu, Scanning Probe-Based Lithography for Production of Biological and Organic Nanostructures on Surfaces, Comprehensive Nanoscience and Technology, Academic Press, 2011, pp. 1–34.
[46] J.A. Heredia-Guerrero, et al., Structural characterization of polyhydroxy fatty acid nanoparticles related to plant lipid biopolyesters, Chem. Phys. Lipids 163 (3) (2010) 329–333.
[47] M. Kwiatkowska, et al., Cutinsomes and lipotubuloids appear to participate in cuticle formation in Ornithogalum umbellatum ovary epidermis: EM–immunogold research, Protoplasma 251 (5) (2014) 1151–1161.
[48] V.G. Correia, et al., The molecular structure and multifunctionality of the cryptic plant polymer suberin, Mater. Today Bio. 5 (2020) 100039.
[49] J.A. Heredia-Guerrero, et al., Sustainable polycondensation of multifunctional fatty acids from tomato pomace agro-waste catalyzed by tin (II) 2-ethylhexanoate, Mater. Today Sustain. 3-4 (2019) 100004.
[50] A. Manrich, et al., Hydrophobic edible films made up of tomato cutin and pectin, Carbohydr. Polym. 164 (2017) 83–91.
[51] A. Montanari, et al., Tomato bio-based lacquer: for sustainable metal packaging, Agro Food Ind. Hi Tech. 25 (2014) 50–54.
[52] G. Tedeschi, et al., Sustainable fabrication of plant cuticle-like packaging films from tomato pomace agro-waste, beeswax, and alginate, ACS Sustain. Chem. Eng. 6 (11) (2018) 14955–14966.
[53] M. Brehm, B. Kirchner, TRAVIS—a free analyzer and visualizer for monte carlo and molecular dynamics trajectories, J. Chem. Inf. Model. 51 (8) (2011) 2007–2023.
[54] O.V.M. Bueno, J.J. Benítez, M.A. San-Miguel, Understanding segregation processes in SAMs formed by mixtures of hydroxylated and non-hydroxylated fatty acids, RSC Adv. 9 (67) (2019) 39252–39263.